Hindawi Publishing Corporation
Advances in Acoustics and Vibration
Volume 2009, Article ID 928367, 17 pages
doi:10.1155/2009/928367

*Research Article*

# A 3D Multiport Scattering Matrix Based-Method for Educing Wall Impedance of Cylindrical Lined Duct Section: Simulation and Error Evaluation

**Mohamed Taktak,[1,2] Jean-Michel Ville,[1] Mohamed Haddar,[2] Gwénaël Gabard,[3] and Felix Foucart[1]**

[1] *Laboratoire Roberval UMR UTC-CNRS no. 6253, Université de Technologie de Compiègne, BP 20529, 60205 Compiègne Cedex, France*
[2] *Unité de Mécanique, Modélisation et Productique (U2MP), Département de Génie Mécanique, Ecole Nationale d'Ingénieurs de Sfax, BP 1173, 3038, Sfax, Tunisia*
[3] *Institute of Sound and Vibration Research, University of Southampton, Southampton SO17 1BJ, UK*

Correspondence should be addressed to Mohamed Taktak, mohamed.taktak.tn@gmail.com

Received 19 December 2008; Revised 16 April 2009; Accepted 29 May 2009

Recommended by Toru Otsuru

The first step to achieve the development of an original indirect method to educe the wall normalized acoustic impedance of a cylindrical lined duct section which includes frequency and modal content pressure field dependence is introduced. It is based on the minimization of the difference between numerical and experimental acoustic power dissipations deduced from the 3D numerical and experimental scattering matrices of a lined duct element. The work presented in this paper is a step toward conducting experiments with a flow duct facility developed during the European DUCAT program. To validate this eduction technique, a simulation of the experiment is performed for no flow conditions assuming an axi-symmetric wall lined with a locally reacting material whose impedance was measured with the two microphone method (TMM). The simulation conducted for two incident pressure vectors with a Monte Carlo's technique also provides an assessment of the uncertainty in three predominant experimental parameters on the scattering matrix coefficients, the acoustic power dissipation, and the educed impedance whose results will be useful during the experiments being conducted.



## 1. Introduction

In many applications such as aircraft engines and ventilation systems, noise produced by sources propagates in presence of mean flow in ducts with large transversal dimensions compared to the wavelength leading to an acoustic pressure field distributed over higher-order modes. To reduce the noise radiated outside by openings, ducts with lined walls are placed in the circuits. To know the impedance of the lined wall is then very important to predict noise with a theoretical modeling. Generally these codes use as an input data, to characterize the lined wall, the acoustic impedance of the material which usually will depend upon frequency, mean flow properties, and pressure field level, more modal content when they are not locally reacting. Moreover, it is known that this lined wall impedance can not depend only on the material property but also on how this material is implemented to constitute the lined duct section. For example, in a cylindrical duct such as aircraft engine inlet the Helmholtz resonator type acoustic material is placed in compartments separated by strips. It has been shown that the mounting conditions of this material and, for example, the presence of intercellular water drain holes can alter the locally reacting property of this material and introduce modal conversions [1, 2]. That is why to handle more realistic aeroacoustic conditions, in addition to the experimental rigs used to measure the impedance of the material, NASA Langley Research Center (NASA LaRC) developed a new technology with microphone and source arrays [3–5] to conduct studies in multimodal propagation

conditions. Recently, after an impedance data comparison acquired from a multiaboratory study [6], NASA LaRC also decided to build a large-scale flow duct that is closer in size, aeroacoustic, and mounting conditions to a full-scale engine to extend the eduction method.

The aim of the work presented in this paper is to develop an indirect technique to measure the "homogenized" impedance of a material averaged on a large lined surface. Also, to ensure results averaged on the modal content of the incident pressure field, studies will be conducted for higher order modes propagation conditions.

Already many works were carried out on indirect methods to measure the acoustic impedance of materials. In fact, because of the progress in the theoretical prediction methods experimental rigs have been constructed to evaluate the properties of materials based on indirect approaches where the liner is ideally placed on the plane surface of a squared duct section allowing studies of the effect of flow on the local acoustic impedance. Several flow duct facilities built in research laboratories assume plane wave incident pressure field leading to easier measurement conditions. For instance, over the last three decades NASA LaRC achieved several test rigs associated to a finite element numerical method for educing the normalized acoustic impedance of a locally reacting liner with an optimization algorithm that minimizes the difference between the measured and theoretical values of the acoustic pressure at the wall facing the liner [7, 8]. This method has since been extended to flow with uniform [9] and shear [10] profiles. Aurégan et al. [11] developed a multimodal theoretical model of the lined duct coupled to a one-dimensional scattering matrix measurement in the hard wall duct section on each side of the lined duct element. A minimization criteria based on the matrix coefficients was performed to educe the impedance. But different liner impedances were found depending on the cost function chosen among the matrix coefficients. Then Elnady and Bodén [12] proposed an analytical mode-matching model of the propagation in the lined section coupled with an experiment to educe the liner impedance. Two cost functions were used: the first is the summation of the differences between the measured and the computed complex pressures at some duct positions; the second is the difference between the measured and calculated complex amplitude of the scattered plane wave. This work was later expanded to include grazing flow effects [13].

The indirect method presented in this paper is based on the minimization of the difference between the measured and numerical acoustic powers dissipated by the whole duct element due to an incident pressure vector. Already a procedure to measure without flow the scattering matrix of a duct section installed in a cylindrical hardware setup was developed [14], and a finite element method presented to compute the theoretical scattering matrix of a cylindrical barrel whose walls are covered with a locally reacting material [15].

In a first step work testing this method, the numerical model will assume no flow, locally reacting wall, and axi-symmetry but the principle of this technique can be applied to more complex situations by extending the theoretical model and the experimental technique to include flow effects, non-axi-symmetric configurations and nonlocally reacting materials. The choice of this simple case will allow to compare the results of the educed impedance with those deduced from the TMM method verifying if the averaged wall impedance equals the local impedance. In addition studies to evaluate the pressure field modal content dependence of the wall impedance can be conducted. Also a homogenized acoustic wall impedance which will fit, for example, the effects of the mounting conditions, can be deduced by calculating the acoustic power dissipations due to an incident equal pressure or equal power vector.

In this paper only stages 2 and 3 of the study which are essential before conducting any experiment are presented in detail:

(1) formulation and calculation of the numerical scattering matrix [15],

(2) development of the eduction technique,

(3) test and evaluation of the method accuracy through a simulation of the experiment,

(4) experiments.

After reminding the general definition of the scattering matrix of a duct element and the physical interpretation of its coefficients, the experimental and numerical methods used to measure and compute the scattering matrix of a lined duct element are described in Section 2. In Section 3, the eduction technique which the liner impedance is based on is presented including the liner dissipation calculation deduced from $[S]$ which is the cost function of the minimization process. The simulation of the experiment is presented in Section 4 with the Monte Carlo's method used to calculate the 95% confident intervals on the scattering matrix coefficients, acoustic power dissipation, and educed normalized impedance.

## 2. Theoretical Basis

*2.1. Definition of the Scattering Matrix of a Lined Duct.* The scattering matrix $[S]$ of a duct element located between the axial coordinates $z_L$ (L meaning left-side) and $z_R$ (R meaning right side) relates the outgoing pressure waves vector $\{P^{\text{out}}\}_{2N} = \langle P_{00}^{I-}(z_L), \ldots, P_{PQ}^{I-}(z_L), P_{00}^{II+}(z_R), \ldots, P_{PQ}^{II+}(z_R)\rangle_N^T$ to incoming pressure waves vector $\{P^{\text{in}}\}_{2N} = \langle P_{00}^{I+}(z_L), \ldots, P_{PQ}^{I+}(z_L), P_{00}^{II-}(z_R), \ldots, P_{PQ}^{II-}(z_R)\rangle_N^T$ (Figure 1) [15, 16]:

$$\begin{aligned}\{P^{\text{out}}\}_{2N} &= [S]_{2N\times 2N} \times \{P^{\text{in}}\}_{2N} \\ &= \begin{bmatrix}[S^{11}]_{N\times N} & [S^{12}]_{N\times N} \\ [S^{21}]_{N\times N} & [S^{22}]_{N\times N}\end{bmatrix}_{2N\times 2N} \times \{P^{\text{in}}\}_{2N}.\end{aligned} \tag{1}$$

The vector $\{P^{\text{in}}\}_{2N}$ contains modal incident pressures $P_{mn}^{I+}(z_L)$ and modal retrograde pressures $P_{mn}^{II-}(z_R)$. The latter is the result of the reflection of the transmitted modal pressures at the open end of the duct. The vector $\{P^{\text{out}}\}_{2N}$ contains modal reflected pressures $P_{mn}^{I-}(z_L)$ and modal

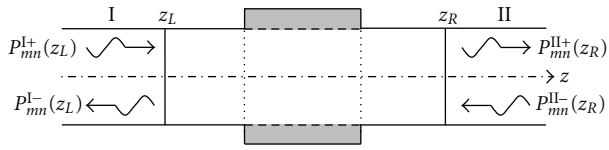


Figure 1: Waves coming in and out of the duct element under test from sides I and II.

transmitted pressures $P^{II+}_{mn}(z_R)$. $N$ is the number of cut-on modes in both cross sections, $P$ and $Q$ being, respectively, the angular and radial wave numbers associated to the $N$th propagating mode. This $2N \times 2N$ matrix represents an intrinsic characterization of the duct element independently of the upstream and downstream acoustic conditions: it depends only on acoustic and geometric features of the duct. The physical meaning of each elementary matrix is as follows:

(i) $[S^{11}_{mn,pq}]_{N\times N}$ the reflection of the wave coming in the element from the left side,

(ii) $[S^{21}_{mn,pq}]_{N\times N}$ the transmission of the wave coming in the element from the left side,

(iii) $[S^{22}_{mn,pq}]_{N\times N}$ the reflection of the wave coming in the element from the right side,

(iv) $[S^{12}_{mn,pq}]_{N\times N}$ the transmission of the wave coming in the element from the right side.

*2.2. Measurement Procedure of the Scattering Matrix.* The simulation of the experiments presented in this paper is performed following the procedure detailed in [14].

*2.2.1. Theory of the Measurement Procedure [14].* The $(2N)^2$ coefficients of $[S]$ are solutions of the system (1). To fill the $2N$ columns of $[P^{\text{out}}]_{2N\times 2N}$ and $[P^{\text{in}}]_{2N\times 2N}$, $2N$ linearly independent modal pressure distributions have to be produced in both cross sections located at $z_L$ and $z_R$. A multiload method was used to improve results [14]. Indeed, tests were carried out with $C$ different loads ($C > 2$) and $N$ source configurations for each load leading to $CN$ linearly independent vectors. The arrangement of the different column vectors results in the construction of the incoming pressures matrix $[P^{\text{in}}]_{2N\times(C\times N)}$ and of the outcoming pressures matrix $[P^{\text{out}}]_{2N\times(C\times N)}$. Finally, the scattering matrix is deduced from the expression:

$$[S]^T = \left[\left[\left[P^{\text{in}}\right]^*\left[P^{\text{in}}\right]^T\right]^{-1}\cdot\left[P^{\text{in}}\right]^*\right][P^{\text{out}}]^T, \qquad (2)$$

where $*$ denotes the complex conjugate.

*2.2.2. Experimental Flow Chart.* The procedure [14] is presented in Figure 2. The study is conducted within the nondimensional frequency band $ka = [0\text{–}3.8]$ leading to $N \leq 5$ modes $((0,0);(\pm1,0);(\pm2,0))$ which can propagate in the main duct. As explained in the previous section, the experiment provides at two cross sections located at $z_L$ and $z_R$ the modal distributions of the incoming and outgoing pressure waves which is achieved by a modal decomposition technique [17, 18] of the total complex pressures measured in two pairs of cross sections $d = 0.05$ m apart located on each side of the test element then separating the incident and reflected modal pressure waves.

Table 1: Source and load configurations $\theta_s$, $r = a$, $z_s$, cylindrical coordinates of the source, and $E_b$ the load length.

| Configuration number | $\theta_s$ (°) | $z_s$ (cm) | $E_b$ (cm) |
|---|---|---|---|
| 1 | 0 | 0 | 0 |
| 2 | 120 | + 15 | 6 |
| 3 | 240 | − 15 | 9 |
| 4 | 8.5 | 0 | 18 |
| 5 | 128.5 | + 15 | 0 |
| 6 | 248.5 | − 15 | 6 |
| 7 | 17 | 0 | 9 |
| 8 | 137 | + 15 | 18 |
| 9 | 257 | − 15 | 0 |
| 10 | 25.5 | 0 | 6 |
| 11 | 145.5 | + 15 | 9 |
| 12 | 265.5 | − 15 | 18 |
| 13 | 34 | 0 | 0 |
| 14 | 154 | + 15 | 6 |
| 15 | 274 | − 15 | 9 |
| 16 | 42.5 | 0 | 18 |
| 17 | 162.5 | + 15 | 0 |
| 18 | 282.5 | − 15 | 6 |
| 19 | 51 | 0 | 9 |
| 20 | 171 | + 15 | 18 |

Being all this procedure repeated for all source configurations and loads [17] chosen to ensure the generation of linearly independent input modal vectors (Table 1); the matrices $[P^{\text{in}}]_{2N\times 2N}$ and $[P^{\text{out}}]_{2N\times 2N}$ are filled by modal coefficients vectors $\{P^{I+}_{mn}(z_L)\}$, $\{P^{II+}_{mn}(z_R)\}$, $\{P^{I-}_{mn}(z_L)\}$, and $\{P^{II-}_{mn}(z_R)\}$. Finally the computation of all the coefficients of the matrix $[S]$ is performed from (2). As only cut-on modes are taken into account, the rank of $[S]$ depends upon the frequency. The influence of the cut-off modes is therefore neglected assuming that $z_L$ and $z_R$ are far enough from the discontinuities at the interface between hard and lined walls.

*2.3. Numerical Computation of the Multimodal Scattering Matrix.* To perform the impedance eduction indirect technique, the theoretical scattering matrix of the duct element is computed with a finite element method detailed in Taktak et al. [15]. This numerical method does not need to solve the FEM equations to determine the pressure distribution into the duct: only relations between incoming and outcoming pressures are constructed to obtain the scattering matrix performing an easier calculation. The theoretical configuration reproduces the experimental duct under test located between $z_L$ and $z_R$ and made of two rigid wall parts, and the lined element (Figure 1) is assumed to be axi-symmetric and covered with a locally reacting material.

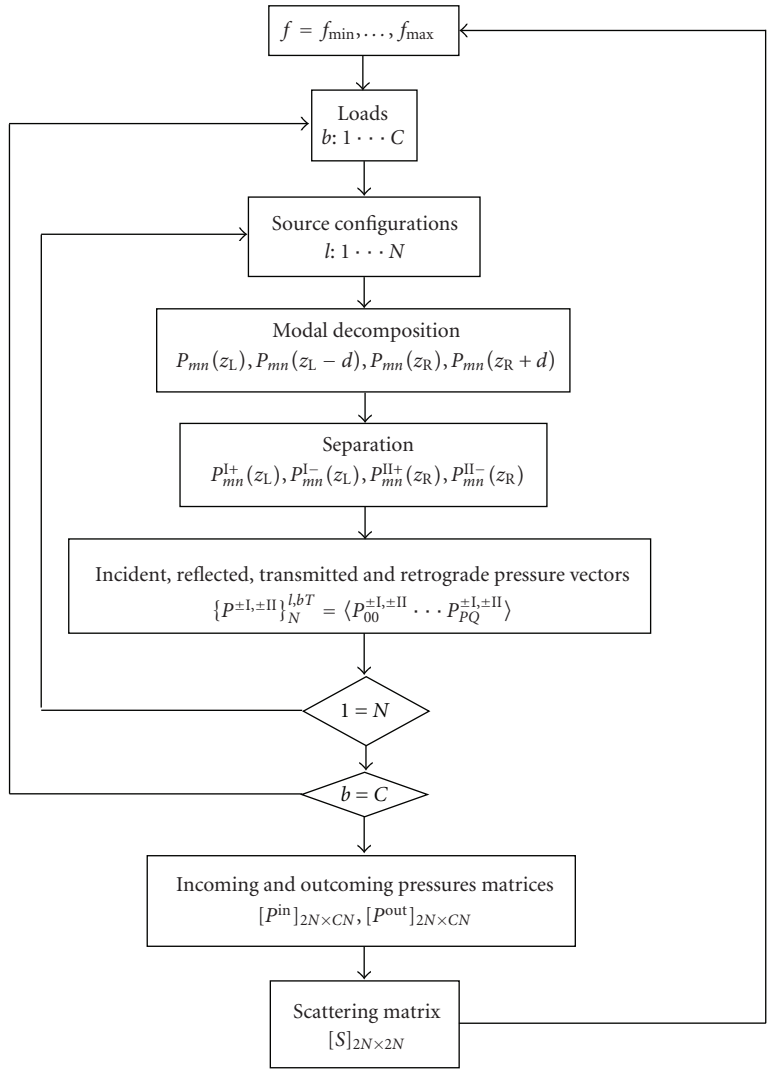


Figure 2: Flow chart of the scattering matrix measurement procedure.

## 3. Determination of the Normalized Acoustic Impedance

The normalized acoustic impedance is deduced by minimizing the cost function defined by the difference between simulated and numerical values of the multiport duct element acoustic power dissipation. After defining the acoustic power dissipation the formulation used to deduce it from the scattering matrix is introduced.

*3.1. Determination of the Acoustic Power Dissipated by the Liner.* The multiport acoustical power dissipation $W_{\text{dis}}$ of a duct element is the difference between the acoustic powers on both sides of the incoming waves $W^{\text{in}}$ and of the outgoing waves $W^{\text{out}}$:

$$W_{\text{dis}} = W^{\text{in}} - W^{\text{out}}. \tag{3}$$

In Taktak et al. [15], it was demonstrated that this acoustic power dissipation can be deduced from

$$W_{\text{dis}}(\text{dB}) = 10\log_{10}\left(\frac{\sum_{i=1}^{2N}(1-\lambda_i)|d_i|^2}{10^{-12}}\right), \tag{4}$$

where $\lambda_i$ are the eigenvalues of the matrix $[S']$ defined by

$$[S']_{2N\times 2N} = [X]_{2N\times 2N}[S]_{2N\times 2N}[X]^{-1}_{2N\times 2N} \tag{5}$$

$[X] = [\text{diag}(\sqrt{N_{mn}k_{mn}/2\rho_0 c_0 k})]_{2N\times 2N}$ $\{d\}_{2N} = [U]^{T*}_{2N\times 2N}$ $\{\Pi^{\text{in}}\}_{2N}$; $\{\Pi^{\text{in}}\}_{2N} = [X_{mn}]_{2N\times 2N}\{P^{\text{in}}\}_{2N}$, $[U]$ is the eigenvectors of the matrix $[S']$; $N_{mn} = SJ_m^2(\chi_{mn})[1 - m^2/\chi_{mn}^2]$ is the normalization factor of mode $(m,n)$ in the hard wall cross sections with $S = \pi a^2$ the duct cross section area, $k_{mn} = \sqrt{k^2 - (\chi_{mn}/a)^2}$ the axial wave number of mode $(m,n)$, $k = 2\pi f/c_0$ ($c_0$ the speed of sound in air and $\rho_0$ the air mass per volume unit), and $\chi_{mn}$ the $n$th root of the first derivative of $J_m$ the Bessel function of the first kind of order $m$. Taktak et

al. [15] pointed out that the overall acoustic power dissipated depends upon the acoustic and geometrical properties of the duct element and upon $\{P^{\text{in}}\}_{2N}$ the incoming pressure waves vector.

*3.2. Indirect Method.* The flow chart of the eduction technique is presented in Figure 3. To avoid divergence of the algorithm, the normalized impedance of the material achieved with the TMM provides an initial value to the iteration process. The educed impedance will then be the result of the minimization of the objective function defined as

$$F_{\text{obj}} = \left| W_{\text{dis Num}}(\text{Watt}) - W_{\text{dis Exp}}(\text{Watt}) \right|. \tag{6}$$

This minimization is performed by the Matlab function "*fminsearch*" based on the Nelder-Mead simplex method [19]. Acoustic power dissipations are deduced from the scattering matrices and the incoming modal pressure vector as shown in the previous section. Then the educed acoustic wall impedance averaged on the length of the liner and on the modal content of the incident acoustic field is deduced.

## 4. Simulation of the Experiment: Procedure

The duct arrangement used for the simulation is presented in Figure 5. The duct element under test located between $z_{\text{L}}$ and $z_{\text{R}}$ is made of two hard wall main ducts and the liner between. On the left-side of this duct element the main duct assumed to be semi-infinite is supporting the source section, and on the right-side a finite length main duct is radiating outside through an infinite baffled open end. Assuming that the duct element under test is defined by its numerical scattering matrix, the total pressures in the four cross sections where the microphones are located are calculated for each source and load configurations listed in Table 1 following the next steps:

(i) determination of the modal incident pressure waves produced by all source configurations,

(ii) calculation of the reflection matrix of the duct open end,

(iii) calculation of the reflected and transmitted waves on each side of the test element.

The data will then pass through the experimental data treatment (Figure 6) leading to the simulated acoustic quantities: scattering matrix, acoustic power dissipation, and educed normalized impedance. The procedure is validated if the simulated scattering matrix is identical to the numerical one.

*4.1. Calculation of Modal Incident Pressures.* A point source whose amplitude $A_s = 1$ and phase $\varphi_s = 0$ is flushed located $(r = a)$ on the main semi-infinite duct wall at its cylindrical coordinates $\theta_s$, $z_s$. The expression of the incident pressure at $z_{\text{L}}$ associated to the mode $(m, n)$ is given by [17]

$$P^{I+}_{mn}(z_{\text{L}}) = \alpha_{mn} A_s e^{j(\varphi_s - m\theta_s + k_{mn}(z_{\text{L}} - z_s))}, \tag{7}$$

where $\alpha_{mn} = 1/2jk_{mn}N_{mn}$. The incident pressure wave vector produced at $z_L$ by the source is given by:

$$\left\{P^{I+}\right\}_N = \begin{Bmatrix} \vdots \\ P^{I+}_{mn}(z_{\text{L}}) \\ \vdots \\ P^{I+}_{pq}(z_{\text{L}}) \\ \vdots \end{Bmatrix}_N = \begin{Bmatrix} \vdots \\ A_s\alpha_{mn}e^{j(\phi_s - m\theta_s + k_{mn}(z_{\text{L}} - z_s))} \\ \vdots \\ A_s\alpha_{pq}e^{j(\phi_s - m\theta_s + k_{pq}(z_{\text{L}} - z_s))} \\ \vdots \end{Bmatrix}_N. \tag{8}$$

If the source is moved at $l = 1, 2, \ldots, M$ different positions (Table 1), then the incident pressure matrix at $z_{\text{L}}$ is obtained as

$$\left[P^{I+}\right]_{N\times M} = \begin{bmatrix} P^{I+,1}_{00}(z_{\text{L}}) & \ldots & P^{I+,l}_{00}(z_{\text{L}}) & \ldots & P^{I+,M}_{00}(z_{\text{L}}) \\ \vdots & \vdots & \vdots & \vdots & \vdots \\ P^{I+,1}_{mn}(z_{\text{L}}) & \ldots & P^{I+,l}_{mn}(z_{\text{L}}) & \ldots & P^{I+,M}_{mn}(z_{\text{L}}) \\ \vdots & \vdots & \vdots & \vdots & \vdots \\ P^{I+,1}_{PQ}(z_{\text{L}}) & \ldots & P^{I+,l}_{PQ}(z_{\text{L}}) & \ldots & P^{I+,M}_{PQ}(z_{\text{L}}) \end{bmatrix}_{N\times M}, \tag{9}$$

where

$$P^{I+,l}_{mn} = A_s\alpha_{mn}e^{j(\varphi_s - m\theta^l_s + k_{mn}(z_L - z^l_s))}. \tag{10}$$

*4.2. Reflection Matrix of an Open End.* The reflection matrix of the infinite baffled open end is deduced from the impedance matrix $[Z^{\text{end}}]_{N\times N}$ as follows [17]:

$$\left[R^{\text{end}}\right]_{N\times N} = \left[[I]_{N\times N} + \left[Z^{\text{end}}\right]_{N\times N}\left[\text{diag}\left(\frac{k_{mn}}{k}\right)\right]_{N\times N}\right]^{-1} \times \left[\left[Z^{\text{end}}\right]_{N\times N}\left[\text{diag}\left(\frac{k_{mn}}{k}\right)\right]_{N\times N} - [I]_{N\times N}\right]. \tag{11}$$

The expression of the impedance matrix $[Z^{\text{end}}]_{N\times N}$ can be approximated by [20]

$$Z^{\text{end}}_{mn,pq} = \begin{cases} 0 & m \neq p \\ \dfrac{2N}{N_{mn}}\left(\displaystyle\int_0^{\pi/2} \sin(\phi) D_{mq}(\sin(\phi)) D_{mn}(\sin(\phi))\, d\phi \right. \\ \qquad \left. - j\displaystyle\int_0^{+\infty} \cosh(\xi) D_{mq}(\cosh(\xi)) D_{mn}(\cosh(\xi))\, d\xi\right), \end{cases} \tag{12}$$

where

$$D_{pq}(\phi) = k\int_0^a J_p(\phi kr) J_p\left(\chi_{pq}\left(\frac{r}{a}\right)\right) r\, dr. \tag{13}$$

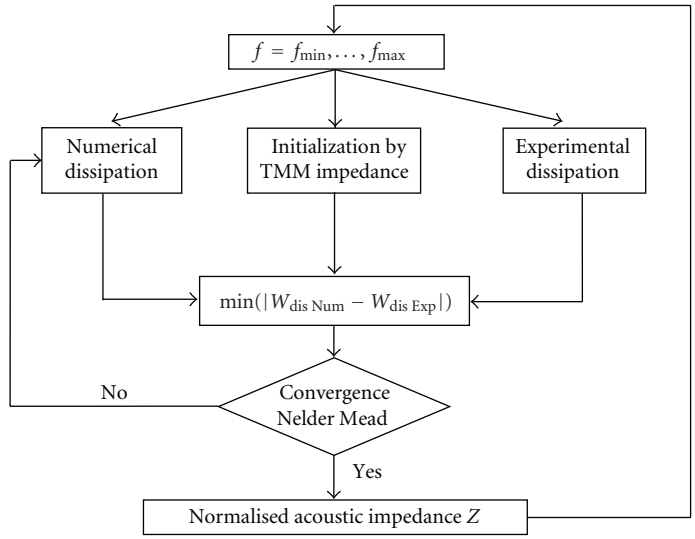


Figure 3: Flow chart of the indirect educed normalized impedance method.

*4.3. Computation of the Reflection and Transmission Matrices.* The transmitted pressure matrix $[P^{II+,b}]_{N\times M}$, the reflected pressure matrix $[P^{I-,b}]_{N\times M}$, and retrograde pressure matrix $[P^{II-,b}]_{N\times M}$ are for the load located at $z_R+E_b$ (Figure 5) given by

$$\begin{aligned}\left[P^{I-,b}\right]_{N\times M} &= \left[R^{I,b}\right]_{N\times N}\cdot\left[P^{I+}\right]_{N\times M},\\ \left[P^{II+,b}\right]_{N\times M} &= \left[T^{b}\right]_{N\times N}\cdot\left[P^{I+}\right]_{N\times M},\\ \left[P^{II+,b}\right]_{N\times M} &= \left[R^{II,b}\right]_{N\times N}\cdot\left[P^{II-,b}\right]_{N\times M},\end{aligned} \tag{14}$$

where $[R^{II,b}]$, $[R^{I,b}]_{N\times N}$, and $[T^b]_{N\times N}$ are, respectively, the reflection matrices at $z_R$ and $z_L$ and the transmission matrix between $z_{\mathrm{L}}$ and $z_{\mathrm{R}}$ whose expressions are given by

$$\begin{aligned}\left[R^{II,b}\right]_{N\times N} &= \left[\operatorname{diag}\left(e^{-jk_{mn}E_b}\right)\right]^{-1}_{N\times N}\\ &\quad\cdot\left[R^{\text{end}}\right]_{N\times N}\cdot\left[\operatorname{diag}\left(e^{jk_{mn}E_b}\right)\right]^{-1}_{N\times N},\\ \left[T^{b}\right]_{N\times N} &= \left[[I]_{N\times N}-[S^{22}]_{N\times N}\cdot\left[R^{II,b}\right]_{N\times N}\right]^{-1}_{N\times N}\\ &\quad\cdot[S^{21}]_{N\times N},\\ \left[R^{I,b}\right]_{N\times N} &= [S^{11}]_{N\times N}+[S^{12}]_{N\times N}\\ &\quad\cdot\left[R^{II,b}\right]_{N\times N}\cdot\left[T^{b}\right]_{N\times N},\end{aligned} \tag{15}$$

where $[S^{11}]$, $[S^{21}]$, $[S^{12}]$, and $[S^{22}]$ are the elementary numerical scattering matrices.

*4.4. Computation of the Transmitted, Reflected, and Retrograde Pressure Vectors.* The total modal pressures at the $z_{\mathrm{L}}$, $z_{\mathrm{L}}-d$, $z_{\mathrm{R}}$, and $z_{\mathrm{R}}+d$, the axial coordinates of the four measurement sections are deduced for all configurations from column vectors of matrices $[P^{I+}]_{N\times M}$, $[P^{I-,b}]_{N\times M}$, $[P^{II+,b}]_{N\times M}$, and $[P^{II-,b}]_{N\times M}$:

$$\begin{aligned}\{P(z_{\mathrm{L}})\}^{b,l}_{N} &= \left\{P^{I+}\right\}^{l}_{N}+\left\{P^{I-}\right\}^{l}_{N},\\ \{P(z_{\mathrm{L}}-d)\}^{b,l}_{N} &= \left[\operatorname{diag}\left(e^{ik_{mn}d}\right)\right]\left\{P^{I+}\right\}^{l}_{N}\\ &\quad+\left[\operatorname{diag}\left(e^{-ik_{mn}d}\right)\right]\left\{P^{I-}\right\}^{l}_{N},\\ \{P(z_{\mathrm{R}})\}^{b,l}_{N} &= \left\{P^{II+}\right\}^{l}_{N}+\left\{P^{II-}\right\}^{l}_{N}\\ \{P(z_{\mathrm{R}}+d)\}^{b,l}_{N} &= \left[\operatorname{diag}\left(e^{ik_{mn}d}\right)\right]\left\{P^{II+}\right\}^{l}_{N}\\ &\quad+\left[\operatorname{diag}\left(e^{-ik_{mn}d}\right)\right]\left\{P^{II-}\right\}^{l}_{N},\end{aligned} \tag{16}$$

where $l$ indicates the source configuration and $b$ the load number (Table 1). These $M$ pressure vectors provide the input data to the procedure described in Figure 2 and Figure 3 leading to the educed impedance.

## 5. Evaluation of the Accuracy of the Normalized Impedance Eduction Technique

Previous studies on the uncertainties in the field of duct acoustic measurements have discussed in detail specific error sources as spectral estimates [21–26], microphone spacing, and locations, providing recommendations to minimize the respective component errors. But few works have been conducted on the propagation of these estimated uncertainties on the overall procedure uncertainties.

Schultz working on methods to extend the frequency range of acoustic impedance testing [26] developed a

systematic framework to estimate uncertainty on reflection factor and impedance. Uncertainty estimation for acoustic data impedance using the two-microphone method (TMM) [27] was made via two ways concluding that the standard analytical technique limited to linear perturbations provides useful scaling information but that the Monte Carlo technique permits propagation of the large uncertainties found in practice. The Monte Carlo technique was also performed to study in a plane wave situation the propagation of source errors on the impedance with the three and four microphone methods [25]. The largest contributors to error were found to be the uncertainties in the magnitude and phase of the pressure transfer functions.

Few works were achieved to estimate the eduction technique uncertainty to determine the acoustic impedance. The accuracy of an analytical-based eduction technique was calculated introducing a random error directly on the coefficients of the transfer matrix [28]. The discrepancy appears at low and high frequencies when a disagreement was already noted between experiment and inverse method. Watson et al. [7] conducted a simulation of their impedance eduction technique including random errors in measurement of sound pressures measured at the wall of a two-dimensional duct that conveys a multimodal sound field. They concluded that for minimizing the effects of these errors on the measurement of the acoustic impedance, more microphones are required. They also discussed the uncertainties of the eduction techniques when measurements conducted with 1980s and 2000s technologies [4] were compared. Deviations up to 1 were pointed out on the normalized impedance for both technologies at or near the antiresonance frequencies of the channel. They concluded to the extreme sensitivity of the educed impedance to measure input parameters which is an issue to all eduction techniques including the standing wave methods.

Few works were done on the propagation of error sources when measurements are performed for higher order mode propagation conditions. In addition to the observations done by Parrott et al. [4] about the 2000s technology, Schultz [27] working on the modal decomposition method (MDM) to measure the impedance versus frequency and mode of a liner placed at the end of a duct and Sitel et al. [14] developing a technique to measure the 3D scattering matrix of a discontinuity carried out studies on uncertainty. Both concluded that results were very sensitive to source errors near the modal cut-on frequency. As in the present study, Sitel et al. [14] used a direct simulation technique of the experiment and the standard analytical technique [26] to propagate deterministic errors in input data as temperature, microphone locations, and the modulus and phase of the modal pressures achieved by a modal decomposition technique [18]. The multiload method was shown to be more reliable than the two load one but unable to measure the coefficients of the matrix associated to wave coming in the duct element after being attenuated by a reactive muffler and reflected by the load. The use of the multisource method was advised to solve this issue.

In the present study the error analysis of the eduction technique involves the simulation of the experiment described in Section 4 and experimental error sources identified by their standard deviations modeled by the generation of perturbations from Gaussian distribution. The Monte Carlo's technique is used to add random perturbations within the uncertainty bounds to error source parameters. In addition to the computation of the scattering matrix, the acoustic power dissipation, and the impedance, the calculation of their 95% confidence intervals is performed.

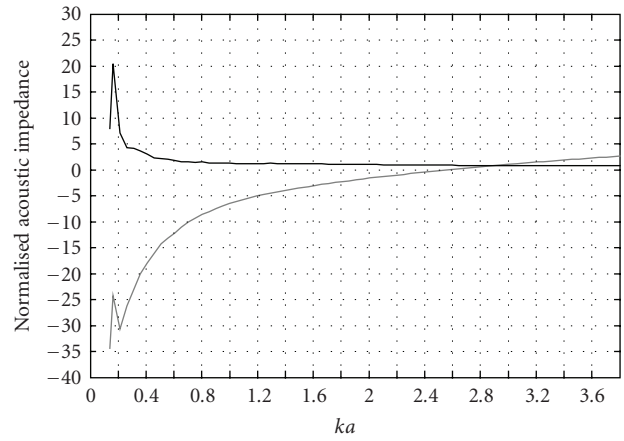


Figure 4: Normalized acoustic impedance of the liner measured with TMM: (black) normalized resistance, (grey) normalized reactance.

*5.1. The Duct Configuration under Test.* The duct element under test located between $z_R$ and $z_L$ (Figure 5) is 1 m long and composed of 3 parts: 0.35 m hard wall duct, 0.3 m lined wall duct, and 0.35 m hard wall duct. It is symmetrical with respect to the duct axis and to the axial centerline. Simulation is conducted for a Helmholtz resonator type liner $L$ made of a perforated plate (thickness $e = 1$ mm, vent diameter $\delta = 1$ mm, and perforation rate $\sigma = 0.025$), a honeycomb (thickness $D = 8$ mm) and backed by a rigid plate (Figure 7) resulting in a nondimensional resonance frequency $ka = 2.6$. The acoustic impedance of the liner plotted in Figure 4 measured with the TMM technique provides an initial value to the eduction process (Figure 3).

*5.2. Parameters of the Study.* To determine error bounds on the eduction technique presented in this paper, a variation of the Monte Carlo's method based on the computation of 10000 iterations as already achieved in a previous work [25] was performed. The propagation of the uncertainty through the data postprocessing which leads to the educed impedance starting at the incident and reflected wave separation step is only concerned. In addition, no error source on the numerical computation of the scattering matrix of the lined duct element is assumed. Only the three following error sources which were already shown to be predominant in the experimental determination of $Z$ [25] by the TMM and of the scattering matrix [14] are taken into account.

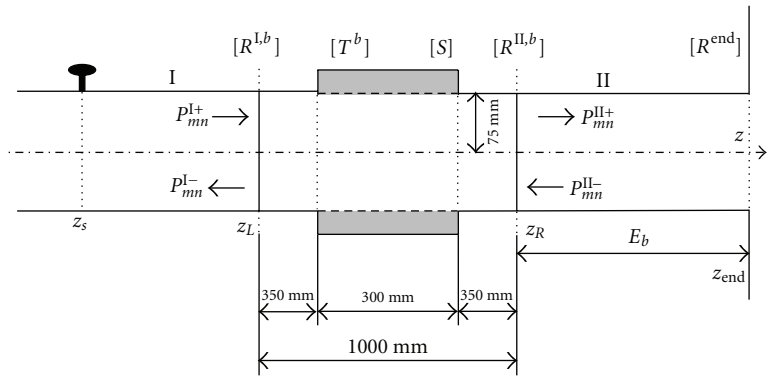


Figure 5: Simulated duct configuration.

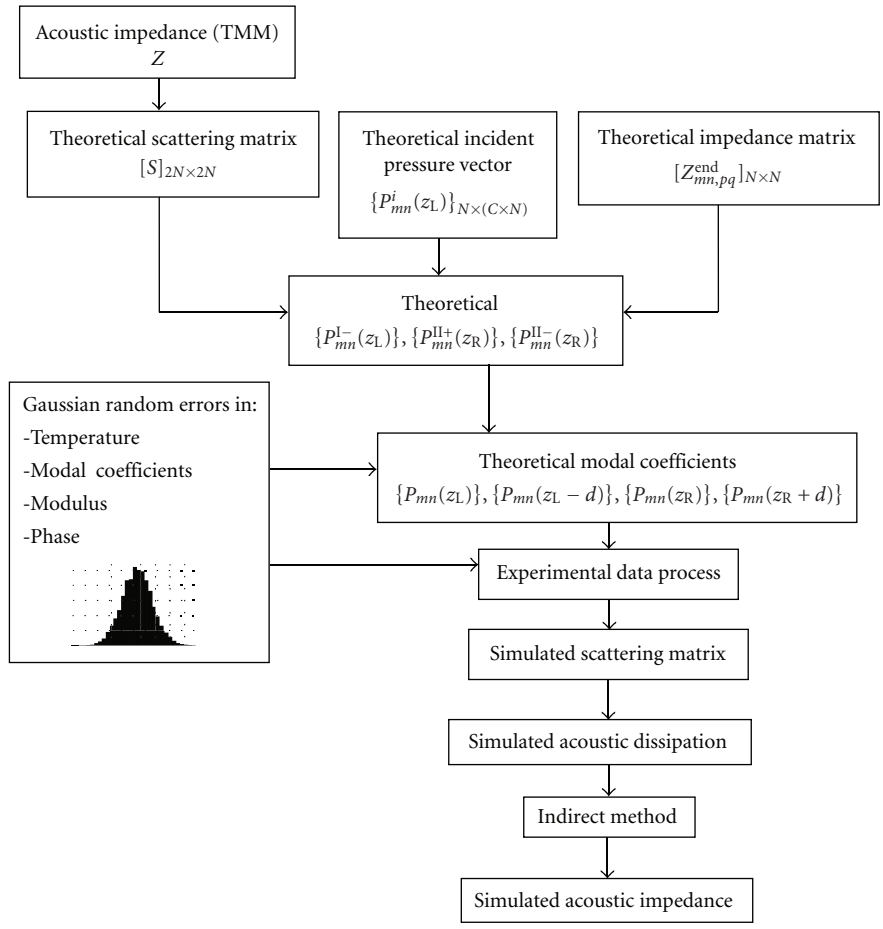


Figure 6: Flow chart of the Monte Carlo's error estimation procedure.

(i) The temperature was shown to be influential when higher order mode propagates [14]. Since a complete experiment can last several days, temperature in the anechoic chamber can vary significantly during the data acquisition process. During an experiment, values of the temperature were stored every second. The standard deviation of the temperature (Table 2) assuming Gaussian distribution was deduced. A typical distribution is shown in Figure 8(a). The lower limit of the frequency range was chosen in order to respect the hypothesis that a mode is cut-on whatever the temperature is.

(ii) The uncertainties in the modulus and phase of the pressure per mode were shown to be predominant for plane wave [25] and higher order modes propagation conditions [14]. The modal decomposition technique which will be performed during

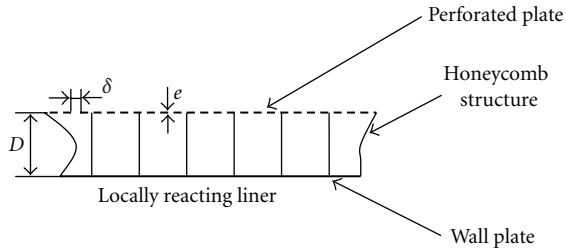


Figure 7: Description of the locally reacting liner.

the experiment and which operates by moving the 4 microphones into 240 positions in the 4 cross sections along the duct radius and by rotating the source along the angular axis was shown [18] to lead to an uncertainty of ±2 dB in the modulus and ±3° in the phase. These values are used to calculate the standard deviation given in Table 2 assuming a Gaussian distribution (Figures 8(b) and 8(c).

*5.3. Results of the Simulation.* In all figures presenting versus *ka* plots of the scattering matrix coefficients, of the acoustic power dissipations and of the educed normalized impedance, the nominal values deduced from the simulation without error and the 95% confidence intervals are displayed. As the nominal educed normalized impedance curves exactly recover those deduced from the numerical and "TMM" methods, this comparison which validates the simulation procedure is not presented. Also as expected, the impedance of the locally reacting liner was verified to be independent of modal content of the incident vector.

*5.3.1. Results and Accuracy of the Scattering Matrix.* The modulus of the scattering matrix coefficients of the duct element under test resulting from the simulation without any error is plotted in Figures 9, 10, and 11 for transmission and in Figures 12, 13, and 14 for reflection of, respectively, modes $(0,0)$, $(1,0)$, and $(2,0)$. Plotted in Figure 9, the plane wave transmission coefficient $|S^{21}_{00,00}|$ decreases as expected with frequency reaching nearly zero around $ka = 2.6$ the resonance frequency of the liner when the reflection coefficients $|S^{11}_{00,00}|$ remains lower than 0.2 in all the frequency domain of the study (Figure 12). The mode $(1,0)$ transmission coefficient $|S^{21}_{10,10}|$ remains closed to zero from $ka = 1.84$, its cut-on frequency to $ka = 2.9$, a frequency higher than the resonance frequency of the liner (Figure 10) then increases with frequency. The mode $(2,0)$ transmission coefficient $|S^{21}_{20,20}|$ is closed to zero near $ka = 3.05$ and increases with the frequency (Figure 11). The reflection coefficients $|S^{11}_{10,10}|$ and $|S^{11}_{20,20}|$ for higher order modes are closed to 1 near their cut-on frequencies and decrease when frequency increases. The conversion coefficients between azimuthal modes in transmission and reflection are not plotted in this paper but were verified to be zero as expected because the axisymmetry of the duct configuration.

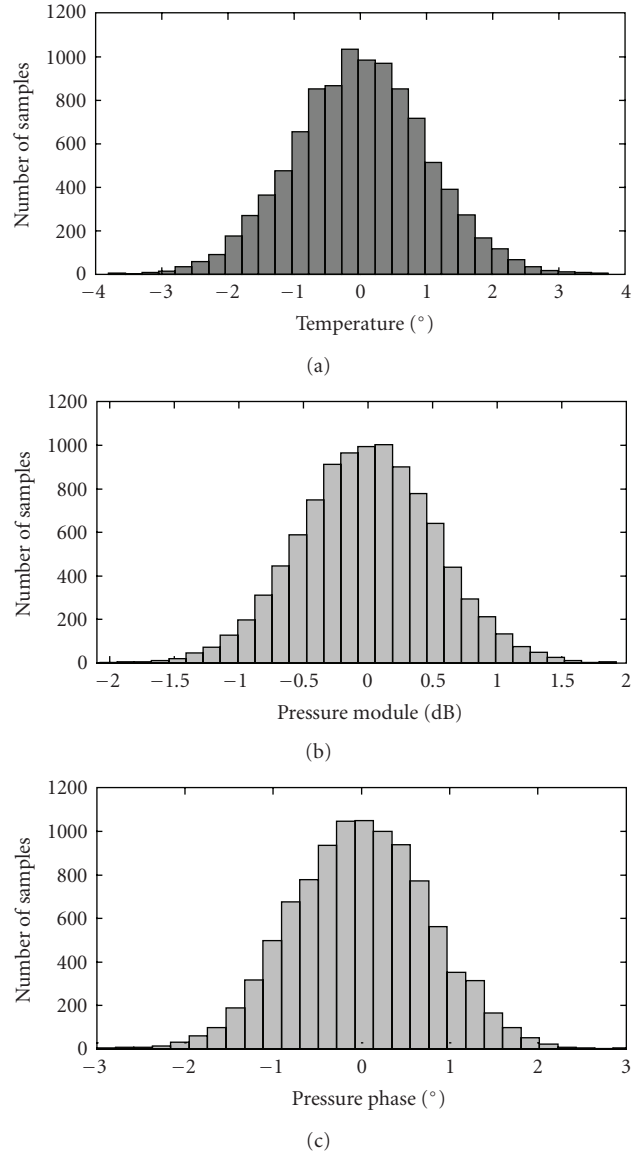


Figure 8: The Gaussian distribution errors used in the simulation process: (a) temperature; (b) total modal pressure module; (c) total modal pressure phase.

(1) *Error in Temperature.* On the same figures as discussed before in Section 5.3.1 (Figures 9–14), the 95% confidence intervals on the scattering coefficients with the uncertainty in temperature are plotted versus *ka*. The 95% confidence interval is very small for all transmission coefficients except for mode $(2,0)$ where it reaches 0.016 near its cut-on frequency (Figure 11). The 95% confidence intervals of the reflection coefficients are small for the plane wave (Figure 12) at all frequencies and equal to 0.83 near the $(1,0)$ mode cut-on frequency (Figure 13) and 1.27 near the $(2,0)$ mode cut-on frequency (Figure 14). In addition, in Figure 14 the distribution of the 10000 samples of $|S^{11}_{20,20}|$ at $ka = 3.08$ where the 95% confidence interval is large points out that near its cut-on frequency the distribution is not Gaussian anymore and that the chance to measure the nominal value

Table 2: Statistical characteristics of errors distributions.

| | Temperature (°C) | Total modal pressure module (dB) | Total modal pressure phase (°) |
|---|---|---|---|
| Standard deviation $\sigma$ | 1 | 0.68 | 0.75 |

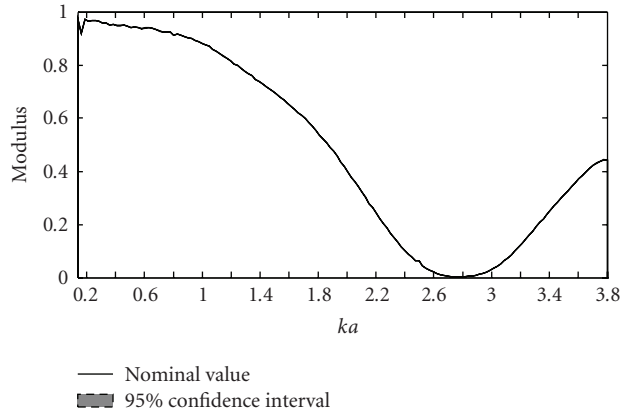


Figure 9: The modulus of the transmission coefficient $S^{21}_{00,00}$ versus $ka$ of the lined duct, with error in temperature.

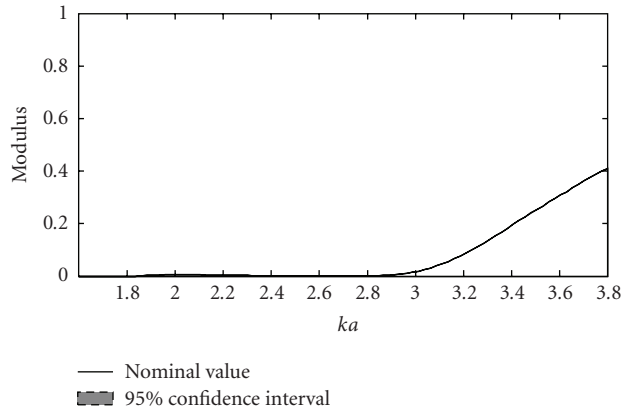


Figure 10: The modulus of the transmission coefficient $S^{21}_{10,10}$ versus $ka$ of the lined duct, with error in temperature.

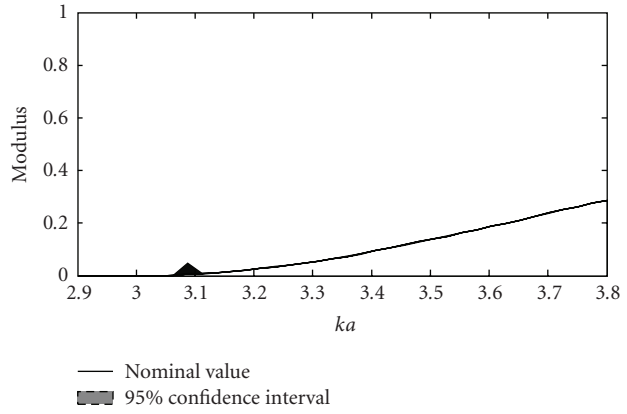


Figure 11: The modulus of the transmission coefficient $S^{21}_{20,20}$ versus $ka$ of the lined duct, with error in temperature.

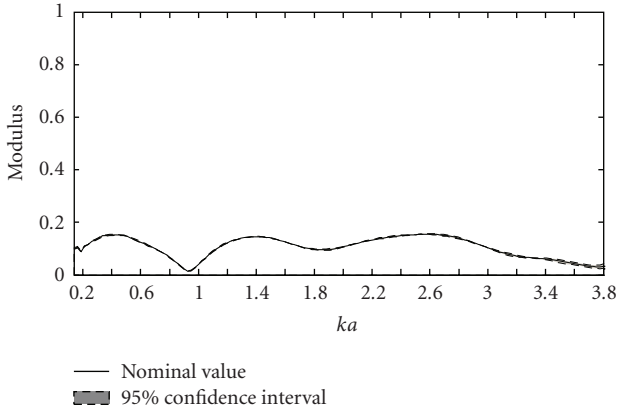


Figure 12: The modulus of the reflection coefficient $S^{11}_{00,00}$ versus $ka$ of the lined duct, with error in temperature.

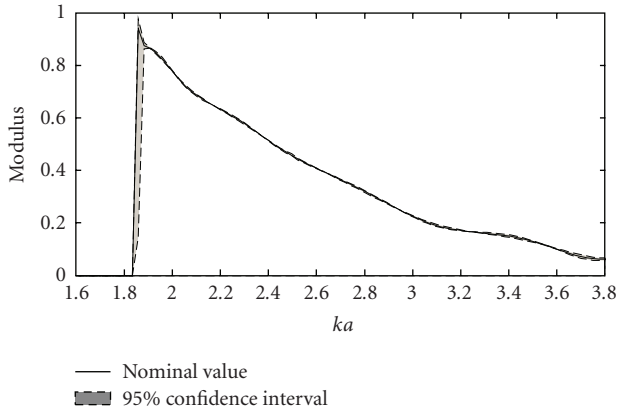


Figure 13: The modulus of the reflection coefficient $S^{11}_{10,10}$ versus $ka$ of the lined duct, with error in temperature.

when an uncertainty in temperature exists is very low. As already pointed out the influence of the error in the temperature on the transmission is shown to be negligible [25] but is predominant on the reflection coefficient of higher order modes near their cut-on frequencies [14].

(2) *Error in the Modulus of the Modal Pressure.* In Figures 15–18 are plotted the 95% confidence intervals versus $ka$ on some scattering matrix coefficients with the uncertainty in the modulus of the modal pressure. Only the transmission coefficient of the plane wave is sensitive to error in the modulus of the modal pressure (Figure 15). The amplitude of the 95% confidence interval of $|S^{21}_{00,00}|$ is very large when $ka < 1.2$ is decreasing when frequency increases. Also the periodicity already observed in a previous work [27] and the dissymmetry of the 95% confidence interval (a

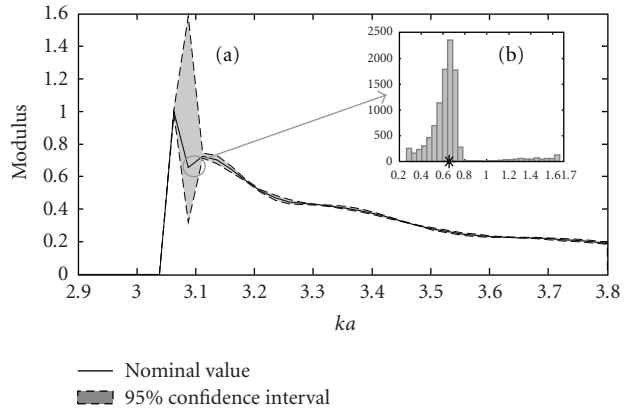


FIGURE 14: (a) The modulus of the reflection coefficient $S^{21}_{20,20}$ versus $ka$ of the lined duct, with error in temperature; (b) statistical distribution and nominal value ($*$) of the modulus of the reflection coefficient $S^{21}_{20,20}$ at $ka = 3.08$.

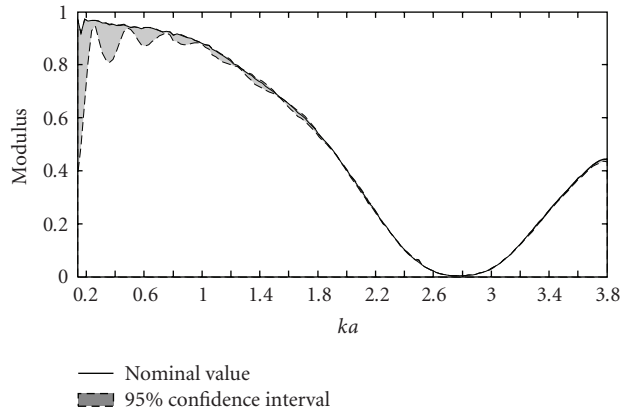


FIGURE 15: The modulus of the transmission coefficient $S^{21}_{00,00}$ versus $ka$ of the duct with the liner, with error in modal pressure modulus.

nominal value different of the median) due to the reflexion on the liner-hard wall duct interfaces and at the open end have to be pointed out. Uncertainties on the reflection coefficient (Figures 16–18) are important whatever the mode is. Indeed the 95% confidence intervals vary between 0.0127 and 0.8264 for $|S^{11}_{00,00}|$ (Figure 16(a)), between 0 and 0.1810 for $|S^{11}_{10,10}|$ (Figure 17), and between 0 and 0.2641 for $|S^{11}_{20,20}|$ (Figure 18), all being more important near the cut-on mode frequencies. As for transmission a dissymmetry and a periodicity of the reflection coefficient distribution are evident. In Figures 16(b) and 16(c) the distributions of the 10000 samples of $|S^{11}_{00,00}|$ at, respectively, $ka = 0.36$ where the nominal value is closed to the median one and $ka = 0.99$ where the nominal value is on the border of the interval are represented. The result of the propagation of the Gaussian distribution remains Gaussian at $ka = 0.99$ while at $ka = 0.36$ the distribution does not follow the normal law although more than a 1/4 of the samples leads to a value closed to the nominal value, increasing the chance to find the exact value.

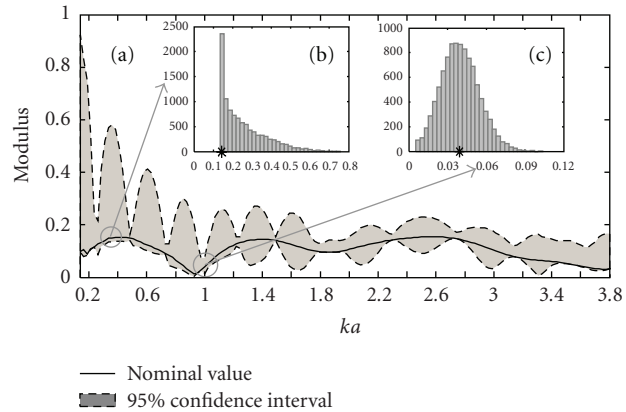


FIGURE 16: (a) The modulus of the reflection coefficient $S^{11}_{00,00}$ versus $ka$ of the duct with the liner, with error in modal pressure modulus; (b) statistical distribution and nominal value ($*$) of the modulus of the reflection coefficient $S^{11}_{00,00}$ at $ka = 0.36$; (c) statistical distribution and nominal value ($*$) of the modulus of the reflection coefficient $S^{11}_{00,00}$ at $ka = 0.99$.

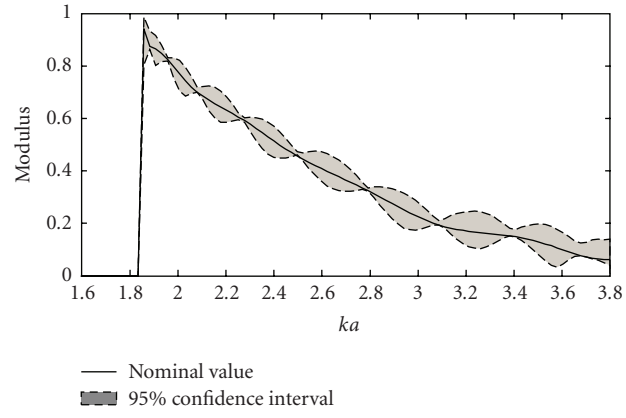


FIGURE 17: The modulus of the reflection coefficient $S^{11}_{10,10}$ versus $ka$ of the duct with the liner, with error in modal pressure modulus.

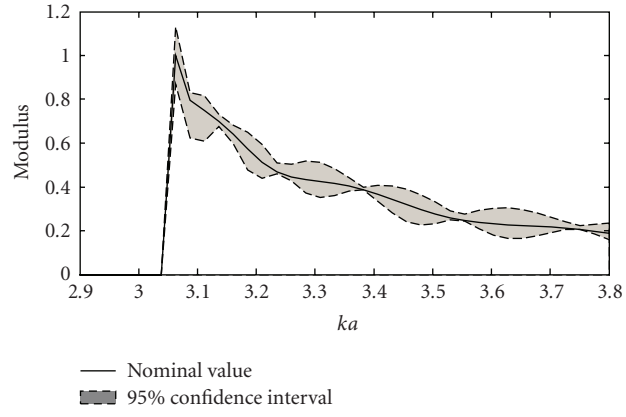


FIGURE 18: The modulus of the reflection coefficient $S^{11}_{20,20}$ versus $ka$ of the duct with the liner, with error in modal pressure modulus.

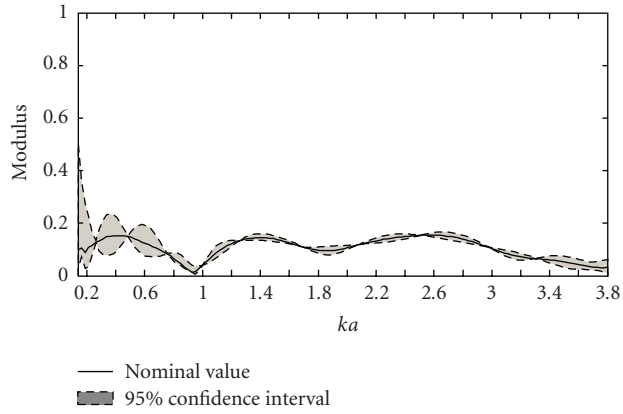


Figure 19: The modulus of the reflection coefficient $S^{11}_{00,00}$ versus $ka$ of the duct with the liner, with error in modal pressure phase.

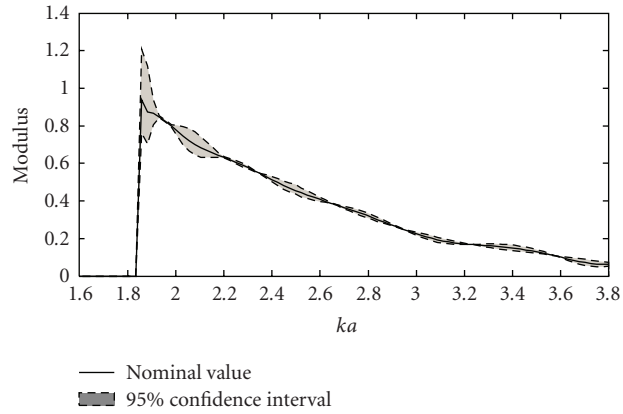


Figure 20: The modulus of the reflection coefficient $S^{11}_{10,10}$ versus $ka$ of the duct with the liner, with error in modal pressure phase.

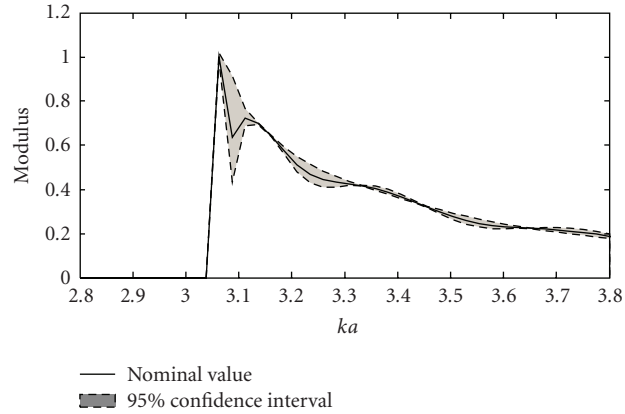


Figure 21: The modulus of the reflection coefficient $S^{11}_{20,20}$ versus $ka$ of the duct with the liner, with error in modal pressure phase.

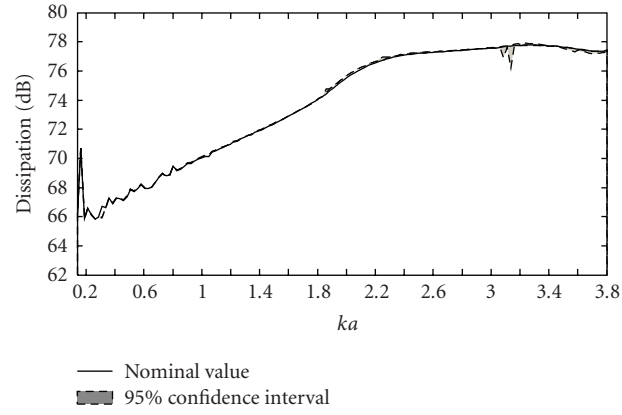


Figure 22: The acoustic power dissipation of the duct with the liner, with error in temperature for the first incoming pressure vector.

(3) *Error in the Phase of the Modal Pressure.* In Figures 19–21 are plotted the 95% confidence intervals versus $ka$ of some scattering matrix coefficients with the uncertainty in the phase of the modal pressure. As this error has a negligible effect on the transmission coefficients, only the results on the reflection coefficient are presented (Figures 19–21). Lower 95% confidence intervals than in the previous Section 5.3.1 (2) are shown. Again the dissymmetry and the periodicity of the 95% confidence interval are still present.

These results show that an improvement in the precision on the scattering matrix measurement can be achieved by working on a better modal decomposition technique and also by performing the separation step in anechoic termination condition with more than two cross sections as suggested in [29].

*5.3.2. Results and Accuracy of the Multiport Acoustic Power Dissipation.* The errors in temperature, modal pressure modulus, and phase studied in the previous section on the scattering matrix will propagate through the procedure leading to the acoustic power dissipation of the lined duct which as demonstrated in Section 3.1 depends not only upon the scattering matrix resulting of the simulation procedure described in Section 4 but also on the incoming modal pressures vector. In this study, two incoming modal pressure vectors were studied: the first $\{P^{\text{in}}\} = \langle 1\,1\,1\,1\,1\,1\,1\,1\,1\,1\rangle^T$ which corresponds to equal amplitude modal pressures incoming in phase from both sides of the lined duct, the second $\{P^{\text{in}}\} = \langle 1\,1\,1\,1\,1\,0\,0\,0\,0\,0\rangle^T$ corresponds to equal amplitude modal pressures incoming in phase from only the left-side of the lined duct. The first vector corresponds to a configuration with a reflective termination and the second with an anechoic termination.

Because the objective function used by the indirect method is based on the acoustic power dissipation (Section 3.2), this study will be helpful to choose the incoming pressure vector leading to the lowest uncertainty on the dissipation.

(1) *First Incoming Pressure Vector.* For the first incoming pressure vector, $W_{\text{dis}}$ (dB), the acoustic power dissipated by the liner increases with frequency from 66 dB reaching a maximum of 78 dB around $ka = 3.2$ slightly higher than the resonance frequency of the liner (Figures 22–24). Also, in

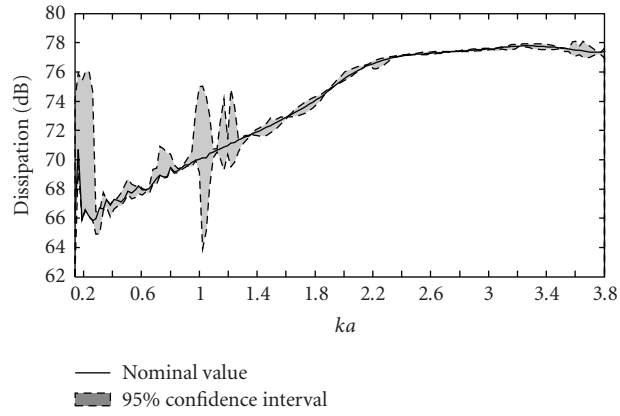


Figure 23: The acoustic power dissipation of the duct with the liner, with error in modal pressure modulus for the first incoming pressure vector.

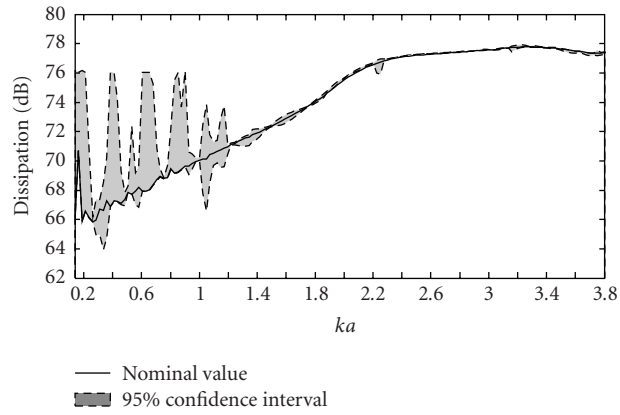


Figure 24: The acoustic power dissipation of the duct with the liner, with error in modal pressure phase for the first incoming pressure vector.

Figures 22, 23, and 24, the 95% confidence intervals on $W_{\text{dis}}$ for uncertainties, respectively, in temperature, modulus, and phase of the total modal pressure are plotted. The influence of the temperature (Figure 22) is shown to be important only near the frequency of the maximum of dissipation. In Figures 23 and 24 the errors in both modulus and phase of the total modal pressure are shown to be amplified during their propagation through the data treatment process leading to very large and dissymmetric 95% confidence interval on $W_{\text{dis}}$ specially for $ka < 1.2$.

(2) *Second Incoming Pressure Vector.* The nominal values of the acoustic power dissipation and its 95% confidence intervals, respectively, for uncertainties in temperature, in the modulus, and phase of the total modal pressure are presented in Figures 25–27 with the second incoming pressure vector. $W_{\text{dis}}$ (dB) the acoustic power dissipated by the liner is shown to be different of this found in the previous section increasing with frequency from 60 dB and reaching a maximum of 75 dB around $ka = 3.4$. The influence of the temperature is pointed out to be important after $ka > 1.82$

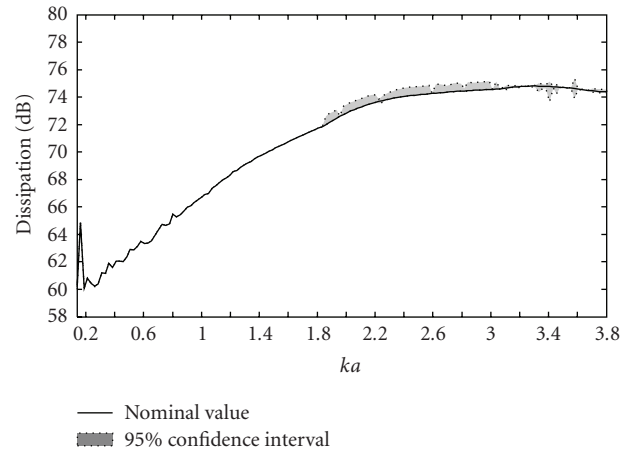


Figure 25: The acoustic power dissipation of the duct with the liner, with error in temperature for the second incoming pressure vector.

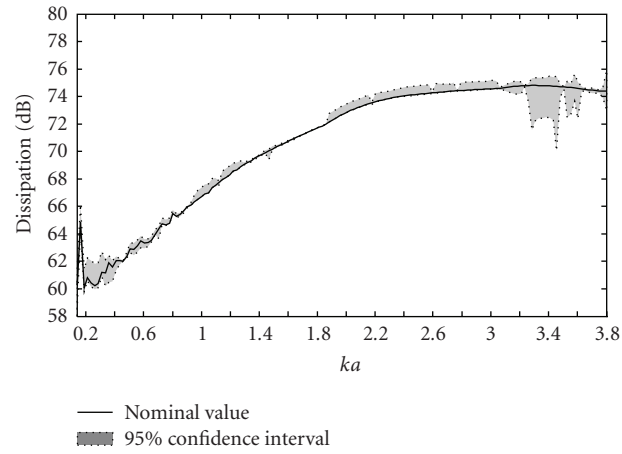


Figure 26: The acoustic power dissipation of the duct with the liner, with error in modal pressure modulus for the second incoming pressure vector.

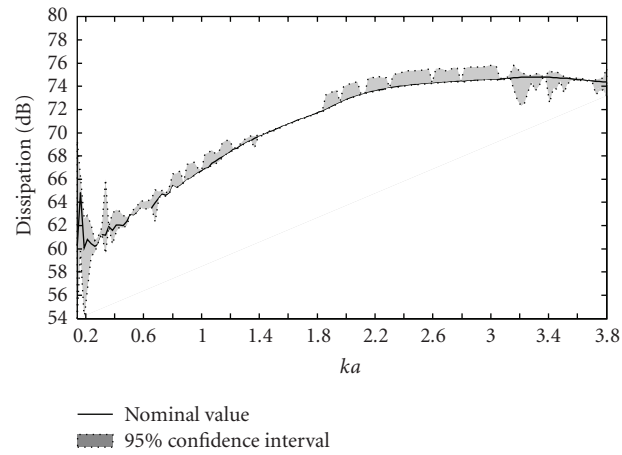


Figure 27: The acoustic power dissipation of the duct with the liner, with error in modal pressure phase for the second incoming pressure vector.

when higher order modes are cut on and especially near the maximum of dissipation with a 1 dB confidence interval for $ka = [1.8–3.8]$.

In Figures 26 and 27 the errors in the modulus and in the phase of the total modal pressure are shown to be present in the all frequency band. But the 15 dB 95% confidence interval pointed out for the first incoming pressure vector in the interval $ka = [0–1.2]$ is reduced between 0.4 and 2 dB for error in modulus and between 0.1 and 6 dB for error in phase. Unlike near the maximum of dissipation the 95% confidence interval in both errors is larger for the second incident vector than for the first one: between 0.1 dB and 6 dB for errors in modulus and between 0 and 1.5 dB for errors in phase.

The comparison between the dissipations calculated for both incoming pressure vectors has pointed out as expected a difference in the acoustic power dissipation values but also a different sensitivity to errors. Results show that the second configuration leads in the all frequency band to a more acceptable uncertainty than the first one whatever the parameters are.

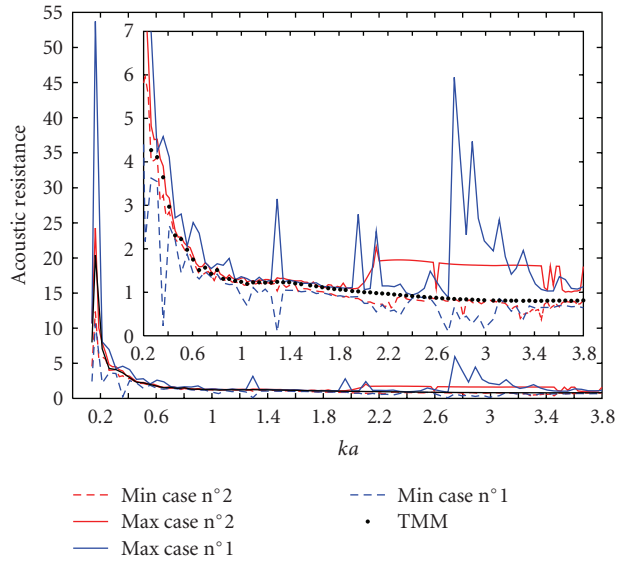


Figure 28: The real part of the normalized educed acoustic impedance. Blue: the first incoming pressure vector, red: the second incoming pressure vector compared to the TMM results.

*5.3.3. Result and Accuracy of the Educed Normalized Impedance.* The real and imaginary parts of the normalized acoustic impedance of the liner deduced from the eduction technique are, respectively, plotted in Figures 28 and 29 versus $ka$ for both incoming pressure vectors. When no error is assumed, the initial values measured with the TMM method are found. The 95% confidence interval on the educed impedance was calculated also with the Monte Carlo's method. But in order to take into account all three error sources together, the Monte Carlo's technique was operated through the simulation procedure to get for each error source 10000 values of acoustic dissipation leading for each frequency to 30000 samples of the acoustic resistance (Figure 28) and reactance (Figure 29).

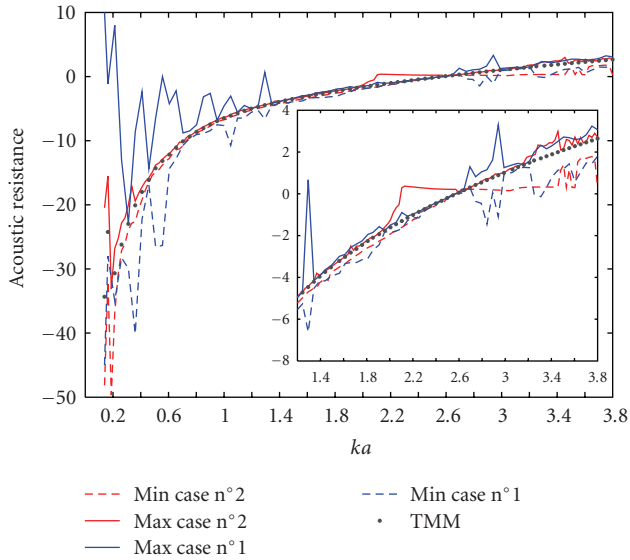


Figure 29: The imaginary part of the normalized educed acoustic impedance. Blue: the first incoming pressure vector, red: the second incoming pressure vector compared to the TMM results.

As expected, for the first incoming pressure vector (case 1), very important errors already observed on acoustic power dissipations in low frequencies $ka = [0.1–1.2]$ and near $ka = [2.2–3.8]$ the maximum of dissipation are also found on the liner impedance: at $ka = 0.168$ the 95% confidence intervals around their nominal values of the acoustic resistance and reactance are, respectively, defined by $11\rho_0c_0 \leq \text{Real}(Z) \leq 54\rho_0c_0$ and $-45\rho_0c_0 \leq \text{Imag}(Z) \leq 10\rho_0c_0$. Near the maximum dissipation frequency $ka = 2.743$, the 95% confidence intervals are narrower than before for the resistance $0.71\rho_0c_0 \leq \text{Real}(Z) \leq 6\rho_0c_0$ and particularly for the reactance $-0.36\rho_0c_0 \leq \text{Imag}(Z) \leq 0.82\rho_0c_0$. In the rest of the frequency domain, the 95% confidence intervals on the acoustic resistance $0.12\rho_0c_0 \leq \text{Real}(Z) \leq 0.75\rho_0c_0$ and on the acoustic reactance $0.05\rho_0c_0 \leq \text{Imag}(Z) \leq 1.15\rho_0c_0$ are small. The results point out that the uncertainties propagate through the impedance calculation procedure without large distortion.

This last remark is also valid for the second incoming pressures vector (case 2) configuration. Indeed, as in Section 5.3.2, the 95% confidence intervals for the resistance $0.01\rho_0c_0 \leq \text{Real}(Z) \leq 0.42\rho_0c_0$ and for the reactance $0.14\rho_0c_0 \leq \text{Imag}(Z) \leq 5.74\rho_0c_0$ are narrow in low frequency $ka = [0.1–1.9]$. As before, near $ka = [2–3.8]$ the frequency of maximum of dissipation, the 95% confidence intervals become larger than with the first incoming pressure vector being $0.01\rho_0c_0 \leq \text{Real}(Z) \leq 2.66\rho_0c_0$ for the acoustic resistance and $0.01\rho_0c_0 \leq \text{Imag}(Z) \leq 2.66\rho_0c_0$ for the acoustic reactance.

To display for both incoming pressure vectors the distribution of the 30000 samples of the acoustic resistance and reactance at $ka = 0.138$ in Figure 30 and at $ka = 2.743$ in Figure 31 (maximum of dissipation) allows to confirm

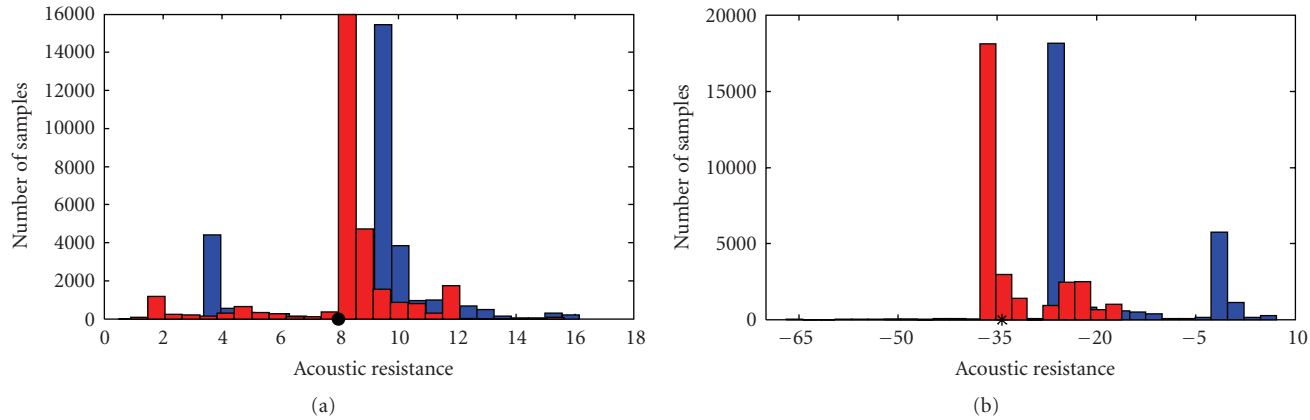


FIGURE 30: (a) distribution of the educed normalized acoustic resistance, (b) distribution of the educed normalized acoustic reactance at $ka = 0.138$. Blue: first configuration, red: second configuration.

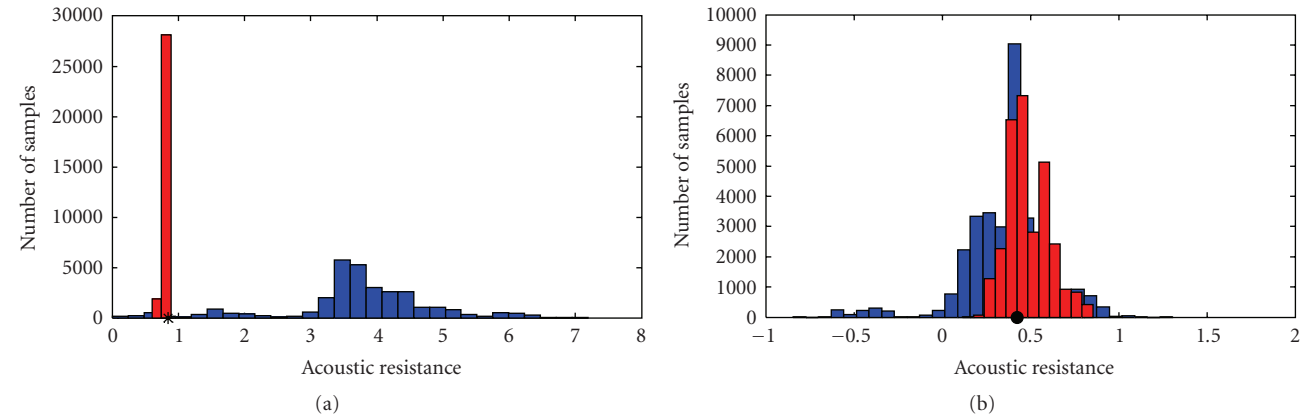


FIGURE 31: (a) distribution of the educed normalized acoustic resistance, (b) distribution of the educed normalized acoustic reactance at $ka = 2.743$. Blue: first configuration, red: second configuration.

the results shown before but also to conduct a more precise analysis. At $ka = 0.138$ for the first case the 95% confidence intervals on acoustic impedance are large ($4\rho_0 c_0 \leq \text{Real}(Z) \leq 16\rho_0 c_0$ and $-45\rho_0 c_0 \leq \text{Imag}(Z) \leq -9\rho_0 c_0$). Moreover the distributions are not Gaussian and lead to a low probability (3% for the resistance and 0.6% for the reactance) to get the exact values of impedance depicted by (•) in figures. For the second case as already discussed the confidence interval is narrower ($1\rho_0 c_0 \leq \text{Real}(Z) \leq 15, 5\rho_0 c_0$) on the resistance but still large $-44\rho_0 c_0 \leq \text{Imag}(Z) \leq -14\rho_0 c_0$ on the reactance. Unlike the first case the distributions are more concentrated around the nominal values showing higher probabilities to get these values: 53% for the resistance and 60% for the reactance. At $ka = 2.743$, near the liner resonance frequency, the second pressure vector leads to narrower 95% confidence intervals than the first one: $0.7\rho_0 c_0 \leq \text{Real}(Z) \leq 0.9\rho_0 c_0$ instead of $0 \leq \text{Real}(Z) \leq 6.7\rho_0 c_0$ and $0.23\rho_0 c_0 \leq \text{Imag}(Z) \leq 0.8\rho_0 c_0$ instead of $-0.6\rho_0 c_0 \leq \text{Imag}(Z) \leq -1.15\rho_0 c_0$. Moreover the probabilities to get the nominal values are very much higher for the second case on the resistance (93% instead of 0.1%) and equal on the reactance (resp., 25% and 30%).

## 6. Conclusions

The 3D acoustic power dissipation deduced from the multiport scattering matrix based-method developed to educe the homogenized impedance of the wall of a cylindrical duct section assumed to be uniform and axi-symmetric has been implemented then validated with a simulation of the whole procedure on a duct configuration ended by an infinite baffle opening.

The Monte Carlo's method was performed with an incident equal pressure vector to calculate the 95% confidence interval in order to study the propagation through the data treatment process of three experimental errors sources on the educed locally reacting impedance of a liner. The study of the propagation of error sources on the scattering and acoustic power dissipation points out that the following.

(i) Error in temperature leads to uncertainty on

(a) only the reflection coefficients of $[S]$ near the cut-on mode frequencies of modes except the plane wave [14],

(b) the acoustic power dissipation near higher order cut-on mode frequencies and becoming more important near the maximum of the dissipation curve located near the cut-on mode frequency of mode $(2,0)$ with 95% confidence intervals larger in the first configuration of incoming modal pressures then the second one.

(ii) Error in the modulus of the modal pressure leads to uncertainty on

(a) the coefficients of $[S]$ in relation with

(1) the transmission only for the plane wave in low frequency domain;

(2) the reflection leading for all modes and $ka$ to a periodic modulation of the 95% confidence interval and being very critical in the low frequency domain ($ka < 0.8$) where only the plane wave propagates;

(b) the acoustic power dissipation for $ka < 0.4$ and $0.9 < ka < 1.2$ for the first configuration in the case of the first configuration of incoming modal pressures. In the second case, these uncertainties are eliminated in low frequencies but they are located in the maximum of dissipation zone with less intensity then the first configuration.

(iii) Error in the phase of the modal pressure leads to uncertainty on

(a) only the coefficients of $[S]$ in relation with the reflection near the cut-on mode frequencies of modes including the plane wave;

(b) the acoustic power dissipation with very large amplitude for $ka < 1.2$.

The analysis of the simulated acoustic impedance results deduced for the two cases of incoming modal pressure vectors showed that the anechoic termination configuration is less sensitive to the uncertainties than the reflective one. This result points out that even the measurement of the scattering matrix was not conducted with an anechoic termination; the choice of an appropriate incident pressure vector will allow to reduce the errors.

The procedure is now being performed during experiments which will be conducted in the UTC's duct flow facility to educe the normalized acoustic impedance averaged on the length of the liner and on the modal content of the incident pressure field of a cylindrical wall duct section covered by a material assumed to be locally reacting. The impedance results will be compared with the TMM results taking into account the 95% confidence interval given by the uncertainty calculation. To point out the pressure field structure dependence of the wall impedance, for example, to mounting and nonuniformity, the influence of the incident pressure field vector will be studied.

The next phases of the study after conducting experiments will be to extend this technique to mean flow conditions, non-axi-symmetric duct section lined by nonlocally reacting materials. These extensions will be made possible by making the experimental and especially the modeling part appropriate.

## References

[1] T. Zandbergen, "Are locally reacting acoustic liners always behaving as they should?" in *Proceedings of the 5th AIAA Aeoroacoustics Conference*, Seattle, Wash, USA, March 1979, AIAA 79-0597.

[2] T. Elnady and H. Bodén, "Mode scattering by hard strips in lined ducts," in *Proceedings of the 10th International Congress on Sound and Vibration*, pp. 621–628, Stockholm, Sweden, July 2003.

[3] M. G. Jones, W. R. Watson, T. L. Parrott, and C. D. Smith, "Design and evaluation of modifications to the NASA Langley flow impedance tube," in *Proceedings of the 10th AIAA/CEAS Aeroacoustics Conference*, vol. 1, pp. 451–463, Manchester, UK, May 2004, AIAA 2004-2837.

[4] T. L. Parrott, M. G. Jones, and W. R. Watson, "Status of duct liner technology for application to aircraft engine nacelles," in *Proceedings of the National Conference on Noise Control Engineering (Noise-CON '05)*, Minneapolis, Minn, USA, October 2005.

[5] M. G. Jones, T. L. Parrott, W. R. Watson, C. H. Gerhold, D. M. Nark, and M. C. Brown, "Development of experimental and computational aeroacoustic tools for advanced liner evaluation," in *Proceedings of the International Congress on Noise Control Engineering (Inter-Noise '06)*, Honolulu, Hawai, USA, December 2006.

[6] M. G. Jones, T. L. Parrott, and W. R. Watson, "Comparison of acoustic impedance eduction techniques of locally-reacting liners," in *Proceedings of the 9th AIAA/CEAS Aeroacoustics Conference and Exhibit*, Hilton Head, SC, USA, May 2003, AIAA 2003-3306.

[7] W. R. Watson, M. G. Jones, S. E. Tanner, and T. L. Parrott, "A finite element propagation model for extracting normal incidence impedance in non-progressive acoustic wave fields," *Journal of Computational Physics*, vol. 125, pp. 177–186, 1996.

[8] W. R. Watson, M. G. Jones, S. E. Tanner, and T. L. Parrott, "Validation of a numerical method for extracting liner impedance," *AIAA Journal*, vol. 34, no. 3, pp. 548–554, 1996.

[9] W. R. Watson, S. E. Tanner, and T. L. Parrott, "Validation of an impedance eduction method in flow," in *Proceedings of the 4th AIAA/CEAS Aeroacoustics Conference*, Toulouse, France, June 1998, AIAA 98-2279.

[10] W. R. Watson, M. B. Tracy, M. G. Jones, and T. L. Parrott, "Impedance eduction in the presence of shear flow," in *Proceedings of the 7th AIAA/CEAS Aeroacoustics Conference*, Maastricht, The Netherlands, May 2003, AIAA 2001-2263.

[11] Y. Aurégan, M. Leroux, and V. Pagneux, "Measurement of liner impedance with flow by an inverse method," in *Proceedings of the 10th AIAA/CEAS Aeroacoustics Conference*, vol. 1, pp. 464–470, Manchester, UK, May 2004, AIAA 2004-2838.

[12] T. Elnady and H. Bodén, "An inverse analytical method for extracting liner impedance from pressure measurements," in *Proceedings of the 10th AIAA/CEAS Aeroacoustics Conference*, vol. 1, pp. 434–450, Manchester, UK, May 2004, AIAA 2004-2836.

[13] T. Elnady, M. Musharrof, H. Bodén, and B. Elhadidi, "Validation of an inverse analytical technique to educe liner impedance with grazing flow," in *Proceedings of the 12th AIAA/CEAS Aeroacoustics Conference*, vol. 5, pp. 3093–3107, Cambridge, Mass, USA, May 2006, AIAA 2006-2639.

[14] A. Sitel, J. M. Ville, and F. Foucart, "Multiload procedure to measure the acoustic scattering matrix of a duct discontinuity for higher order mode propagation conditions," *Journal of the Acoustical Society of America*, vol. 120, no. 5, pp. 2478–2490, 2006.

[15] M. Taktak, J. M. Ville, M. Haddar, G. Gabard, and F. Foucart, "Acoustic liners behavior investigation using the multimodal scattering matrix," *International Review of Mechanical Engineering*, vol. 2, no. 4, pp. 566–576, 2008.

[16] R. T. Muehleisen and D. C. Swanson, "Modal coupling in acoustic waveguides: planar discontinuities," *Applied Acoustics*, vol. 63, no. 12, pp. 1375–1392, 2002.

[17] M. Akoum and J. M. Ville, "Measurement of the reflection matrix of a discontinuity in a duct," *Journal of the Acoustical Society of America*, vol. 103, no. 5, pp. 2463–2468, 1998.

[18] J. M. Auger and J. M. Ville, "Measurement of liner impedance based on the determination of duct eigenvalues by a Fourier-Lommel's transform," *Journal of the Acoustical Society of America*, vol. 88, no. 1, pp. 19–22, 1990.

[19] J. C. Lagarias, J. A. Reeds, M. H. Wright, and P. E. Wright, "Convergence proprieties of the Nelder-Mead simplex method in low dimensions," *SIAM Journal of Optimization*, vol. 9, no. 1, pp. 112–117, 1998.

[20] W. E. Zorumski, "Generalized radiation impedances and reflection coefficients of circular and annular ducts," *Journal of the Acoustical Society of America*, vol. 54, no. 6, pp. 1667–1673, 1973.

[21] H. Bodén and M. Åbom, "Influence of errors on the two-microphone method for measuring acoustic properties in ducts," *Journal of the Acoustical Society of America*, vol. 79, no. 2, pp. 541–549, 1986.

[22] M. Åbom and H. Bodén, "Error analysis of two-microphone measurements in ducts with flow," *Journal of Acoustical Society of America*, vol. 83, no. 6, pp. 2429–2438, 1988.

[23] A. F. Seybert and B. Soenarko, "Error analysis of spectral estimates with application to the measurement of acoustic parameters using random sound fields in ducts," *Journal of the Acoustical Society of America*, vol. 69, no. 4, pp. 1190–1199, 1981.

[24] B. F. G. Kaltz, "Method to resolve microphone and simple location errors in the two-microphone duct measurement method," *Journal of Acoustical Society of America*, vol. 108, pp. 2231–2237, 2000.

[25] R. T. Muehleisen and C. W. Beamer IV, "Comparison of errors in the three- and four-microphone methods used in the measurement of the acoustic properties of porous materials," *Acoustic Research Letters Online*, vol. 3, no. 4, pp. 112–117, 2002.

[26] T. Schultz, M. Sheplak, and L. N. Cattafesta III, "Uncertainty analysis of the two-microphone method," *Journal of Sound and Vibration*, vol. 304, no. 1-2, pp. 91–109, 2007.

[27] T. Schultz, *Acoustic impedance testing for aeroacoustic applications*, Ph.D. thesis, University of Florida, Gainesville, Fla, USA, 2006.

[28] M. Leroux, *Propagation acoustique en conduit traité: influence de l'écoulement sur la propagation avec impédance de paroi*, Ph.D. thesis, Université du Maine, Le Mans, France, 2005.

[29] A. Sitel, *Méthodes de mesure des matrices acoustiques des discontinuités à un ou deux ports en présence des modes élevés*, Ph.D. thesis, Université de Technologie de Compiègne, Compiègne, France, 2005.